

Analysis of en échelon/hackle fringes and longitudinal splits in twist failed glass samples by means of fractography and electromagnetic radiation

Vladimir Frid^{a,*}, Dov Bahat^a, Avinoam Rabinovich^{b,1}

^aDepartment of Geological and Environmental Sciences, Ben Gurion University of the Negev, PO Box 653, Beer Sheva, 84105 Israel

^bPhysics Department, The Deichmann Rock Mechanics Laboratory of the Negev, Ben Gurion University of the Negev, POB 653, Beer Sheva, 84105 Israel

Received 7 March 2003; received in revised form 10 May 2004; accepted 10 May 2004

Available online 11 September 2004

Abstract

This study introduces several innovations in the experimental study of fracture. (1) A new method of simulating fringe cracks; this is accomplished by the application of uniaxial compression on cylinders that contain out-of-plane pre-cuts along their walls. Previous investigators combined independent operations of mode III to mode I, whereas in the present experiment, a single remote compression was transformed into mixed modes I and III by local stress rotation along the pre-cuts. An enlargement of inter pre-cut angle causes an increase of sample strength. (2) Contrary to previous experiments and many field exposures in sediments that exhibit transitions from parent fractures to fringes, the present study simulates a reverse transition, from fringes to parent fractures (to tensile longitudinal (axial) splits). Thus, a change occurs from local mixed modes I and III to local single mode I. The new results may be applied to the interpretation of secondary fractures and fringes in naturally fractured granites. (3) Monitoring of the electromagnetic radiation (EMR) that was induced by the fractured samples enabled us to determine in real time, the sequence of events and the fracture velocities along the various failure stages. Strings of high-frequency EMR pulses (with a frequency of several MHz) were measured during the fringe formation, indicating small widths of en échelon cracks, while the subsequent longitudinal splitting initiated lengthy EMR pulses of lower frequency (some tens of kHz) indicating much wider cracks (which indeed were measured).

© 2004 Elsevier Ltd. All rights reserved.

Keywords: En échelon fringes; Axial split; Electromagnetic radiation induced by fractures

1. Introduction

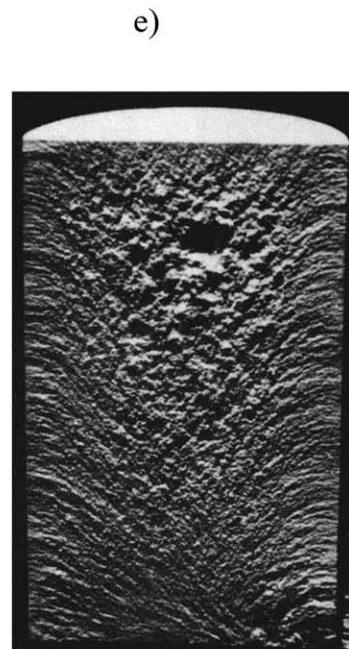
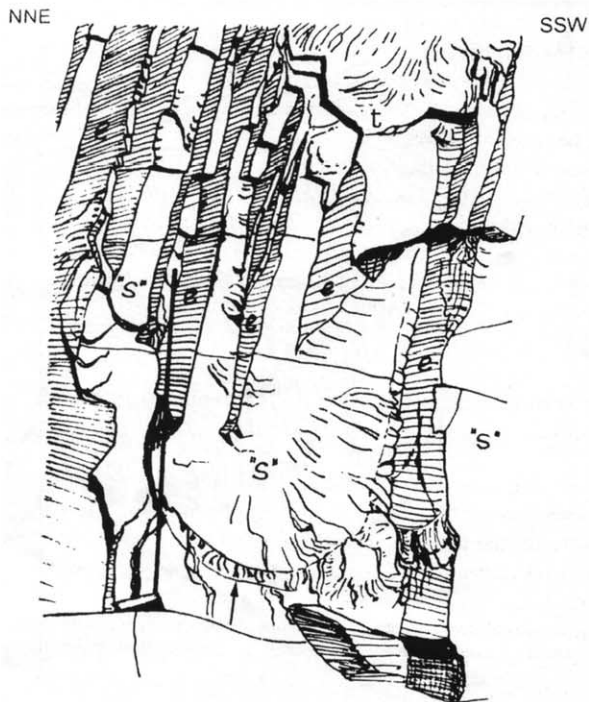
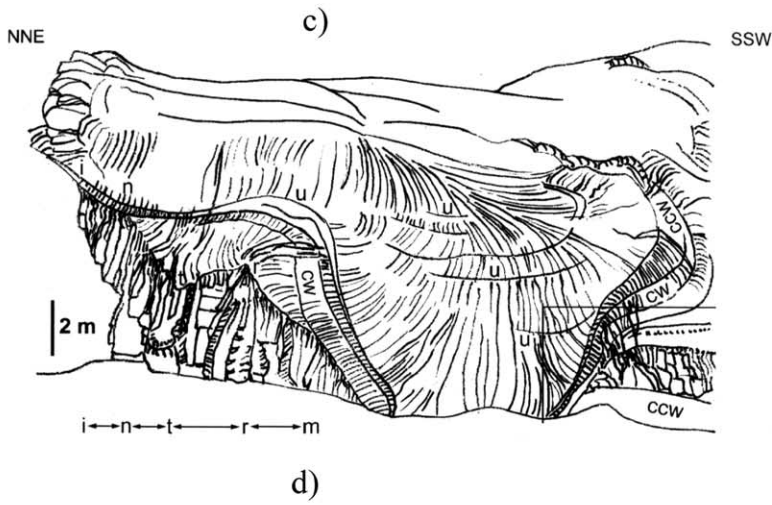
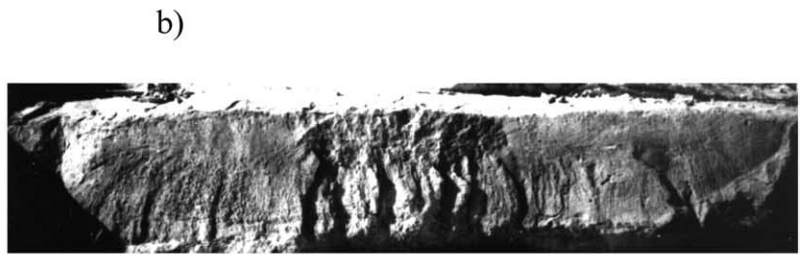
1.1. Geological background

Fractures are among the most common of all geological features (Twiss and Moores, 1992, p. 37) and joints probably are more common than other fractures. A typical joint surface consists of a parent joint marked by plumes that indicate the direction of fracture propagation and two fringes that form above and below it (Fig. 1a). Each fringe consists of a series of alternating en échelon cracks (also termed segments) and steps (also termed bridges) that are aligned along the parent joint. The parent joint registers

early processes in the fracture history, while the fringes record late events in this history. There exist, however, some discordant findings regarding fracture processes on parent joints and joint fringes. For instance, in Fig. 1a is found an en échelon segment, which starts from a 'shoulder', far from the center of some parent joints whereas in different occurrences the segment initiates around the joint center. Furthermore, there are (at least) two variations of plume structures. In the more common variation an early plume appears on the joint surface and arrests at the shoulder and new plumes grow individually on the en échelon cracks, as shown in the classic model by Hodgson (1961). There is strong evidence that some en échelon fringes develop in a later, separate event from the parent joint (Bahat, 1986, 1997; Younes and Engelder, 1999). The less common variation is that of a continuation of parts of the plume from the parent joint to the en échelon cracks (e.g. Bankwitz, 1965, Fig. 8), with the implication that the parent joint and

* Corresponding author. Tel.: +972-7-6461-770; fax: +972-7-6472-997
E-mail address: vfrid@bgumail.bgu.ac.il (V. Frid).

¹ The Deichmann Rock Mechanics Laboratory of the Negev, Ben Gurion University of the Negev, POB 653, Beer Sheva, 84105 Israel.



en échelon segment were formed in a single continuous process (Fig. 1b). Another issue concerns multiple segment styles on a single joint, where the segment in the upper fringe differs from the segment in the lower one (Fig. 1a), suggesting a complex, multistage fracture process. Particularly intriguing are recent discoveries of joints cutting granites that display wide varieties of interrelations between parent joints (mirror planes) and fringes (Fig. 1c and d). These complex fracture surface morphologies exhibit alternating parent joints and fringes, indicating that under intense fracture conditions mirror planes can mimic parent joints on fringes on the same fracture surface (Bahat et al., 2001a, 2002).

1.2. Previous fracture experiments

The few examples mentioned above demonstrate that fracture markings on joint surfaces indicate complex fracture histories that need to be deciphered in order to improve our understanding of processes in fracture geology. While the parent joint clearly forms by a mode I (opening) loading, an en échelon segment reflects a more complex fracture process by mixed modes I and III (e.g. Pollard et al., 1982). Much of the present understanding of processes in structural geology is drawn from experimental results. An interesting simulation of the mode I parent joint was experimented by Gramberg (1965). He induced axial splitting in cylindrical specimens of fine-grained brittle rock (one example was specified as lithographic limestone) by both uniaxial and diametral compression. The plumes obtained on the longitudinal (axial) splitting revealed that the fracture origin was at the corner of the fracture plane, i.e. at the sample tip, and the joint plane was divided into a central ragged wedge, and wavy plumes on both sides curving towards the sample walls (Fig. 1e). No fringe cracks were formed by this experiment. In contrast, two inducements of en échelon segments were performed on glass and polymethyl methacrylate (PMMA) by Sommer (1967, 1969) and Cooke and Pollard (1996), respectively. The latter two studies broadened significantly our understanding of en échelon formation, but they did not add information on axial splits. Our experiment combines the simulation of these two structure styles by a single loading.

1.3. Electromagnetic radiation (EMR)

We consider only EMR in the frequency range from 1 kHz

to 50 MHz. EMR from materials fractured under compression was first observed by Stepanov in 1933 on samples of sylvine (KCl) (Urusovskaja, 1969). This investigation was followed by numerous others, which measured EMR from a very wide range of piezo- and non-piezoelectric, crystalline and amorphous, metallic and non-metallic materials and rocks under different stress loadings (Nitsan, 1977; Warwick et al., 1982; Khatiahvili, 1984; Ogawa et al., 1985; Cress et al., 1987; Yamada et al., 1989; O'Keefe and Thiel, 1995; Ueda and Al-Damegh, 1999; Bahat et al., 2004).

Here, we only briefly summarize some known experimental results:

- An increase of elasticity, strength, and loading rate during uniaxial loading increases EMR amplitude (Gol'd et al., 1975; Nitsan, 1977; Khatiahvili, 1984).
- The key elastic parameter for EMR characterization during triaxial compression is the Poisson ratio. The lower the Poisson ratio, the higher the EMR activity (Frid et al., 1999).
- An individual EMR pulse amplitude, $A(t)$, can be characterized by the following general relationship (Rabinovitch et al., 1998):

$$A = \begin{cases} A_0 \sin(\omega(t - t_0))(1 - \exp(-(t - t_0)/\tau)), & t < T \\ A_0 \sin(\omega(t - t_0))\exp(-(t - T)/\tau)(1 - \exp(-(T - t_0)/\tau)), & t \geq T \end{cases} \quad (1)$$

The envelope of the pulse is of the form:

$$\begin{cases} A_0(1 - \exp(-(t - t_0)/\tau)), & t < T \\ A_1(-\exp(-(t - T)/\tau)), & t \geq T \end{cases} \quad (2)$$

where $A_1 = A_0(1 - \exp(-(T - t_0)/\tau))$. This envelope is marked on Fig. 2 by a dashed line.

In Eqs. (1) and (2), t is the time, t_0 is the time from the origin up to the pulse beginning, and T is the time from the origin up to the EMR pulse envelope maximum. Thus, $T' = T - t_0$ is the time interval to reach pulse maximum, $\tau_1 = \tau_2 = \tau$ is the rise time and the fall time (RFT), which are identical within experimental uncertainty, ω is the frequency, and A_0 is the pulse peak amplitude. Important parameters are shown in Fig. 2. Thus, (i) the rise time τ_1 is connected with the initial slope of the graph and is actually the time it takes the tangent to the curve, at its inception, to

Fig. 1. (a) A fracture cutting Lower Eocene chalk in the Shephela syncline, central Israel. En échelon fringes occur on both the upper and lower sides of the parent joint. There is a clockwise rotation of the en échelon segments with respect to the parent joint in the upper fringe and a counterclockwise rotation in the lower one. Cracks in the two fringes differ considerably in shape. Segments are dark and steps are light. Width of the parent joint is about 20 cm (after Bahat, 1997). (b) The 'curved-joint' showing an en échelon segment below the elliptical perimeter of the early 'embryonic' joint at center. The joint undulates along the strike. The delicate barbs on the joint surface represent a bilateral plume. The width of the parent joint is about 40 cm (after Bahat, 1997). (c) A drawing of a joint cutting granite from the South Bohemian Pluton in the Czech Republic displaying the edge of the parent joint, also termed primary mirror plane, and a complex fringe below (after Bahat et al., 2001a); u, cw and ccw are undulations, clockwise and counterclockwise, respectively. The vertical scale at the left of the SM is 2 m (after Bahat et al. 2001a). (d) The fringe from (c) contains multiple fractures: Surfaces of the tensile en échelon segments and shear steps are marked by e and 's', respectively. The large 's' at center (at t) is a secondary parent joint, also termed secondary mirror (SM) plane, which contains a secondary fringe at its lower part (marked by a vertical arrow). (e) Axial split induced by diametral compression (Brazilian tensile test) in a cylindrical rock sample 30 mm in diameter, showing two curved plumes initiating in the fracture origin and fanning away from each other (modified from Gramberg, 1965).

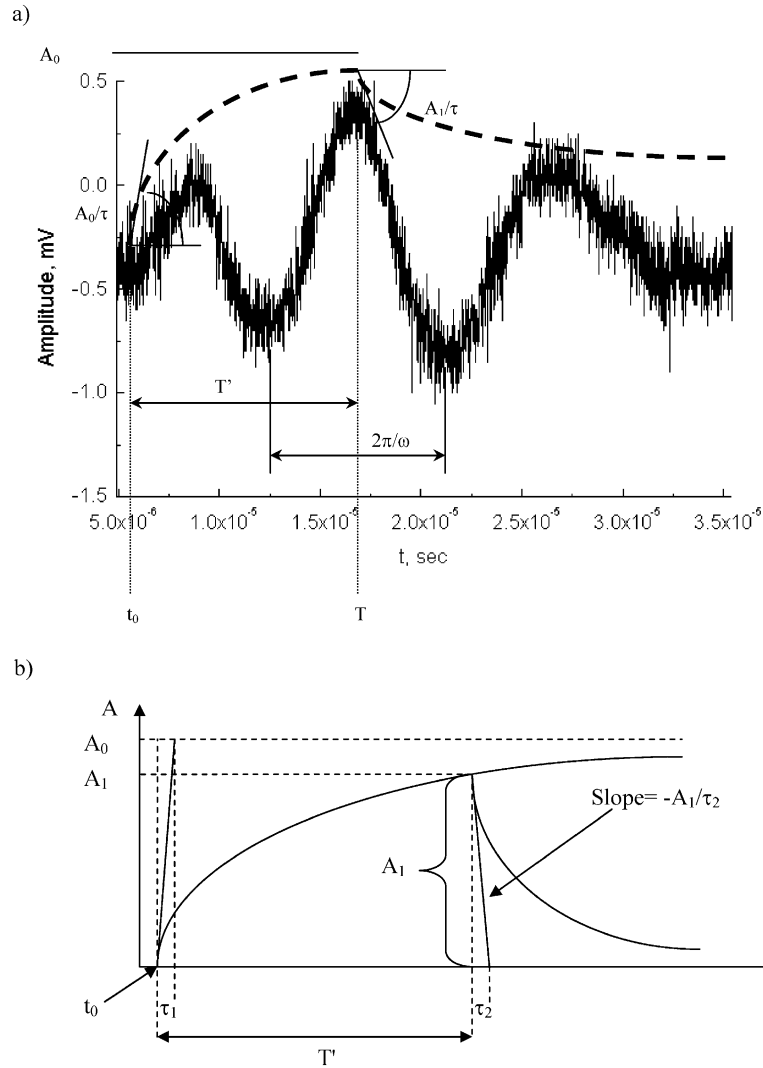


Fig. 2. (a) A lengthy EMR pulse, EMR pulse envelope (dashed line) and definition of EMR parameters from Eqs. (1) and (2) (see Section 1.3). (b) Schematic diagram of EMR envelope including parameters definition.

reach the maximum height; (ii) A_0 is the ultimate, unattainable, maximum amplitude that would have been reached had the propagation time continued indefinitely; (iii) T' is the actual crack propagation time and the EMR envelope increase time: after T' time units from its beginning, the EMR pulse has reached its (attainable) maximum amplitude A_1 ; (iv) τ_2 is the decay time and is again related to the initial (falling) slope at $t - t_0 = T'$. This slope is $-A_1/\tau_2$. In our experiments as well as in our theory (Frid et al., 2003; Rabinovitch et al., 2003), $\tau_1 = \tau_2$. All the parameters A_0 , T' , ω and τ (Fig. 2) can be calculated by a least squares fit (Rabinovitch et al., 1998) to the experimental results.

(d) The EMR pulse amplitude ‘A’ increases in absolute value as long as the crack continues to grow, when new atomic bonds are severed and their contribution is added to the EMR (Rabinovitch et al., 1998, 2000a,b,c; Frid et

al., 2000). Hence, A_1 should depend on crack area (Frid et al., 2003).

(e) Concomitantly T' , the time from the pulse origin to the maximum of its envelope, is proportional to the crack length ℓ (assuming the crack velocity ‘ v_{cr} ’ to be almost constant) (Rabinovitch et al., 1998; Bahat et al., 2001b):

$$T' = \frac{\ell}{v_{cr}} \tag{3}$$

The assumption of constant velocity of the crack is obviously an abstraction since the crack initially accelerates and finally decelerates to a halt. However, since the acceleration and deceleration times are short with respect to T' (Fineberg and Marder, 1999) they are neglected.

(f) The frequency ω of the EMR pulse is related to the crack width ‘ b ’ (Rabinovitch et al., 1998, 1999). Assuming that the wavelength of the atomic

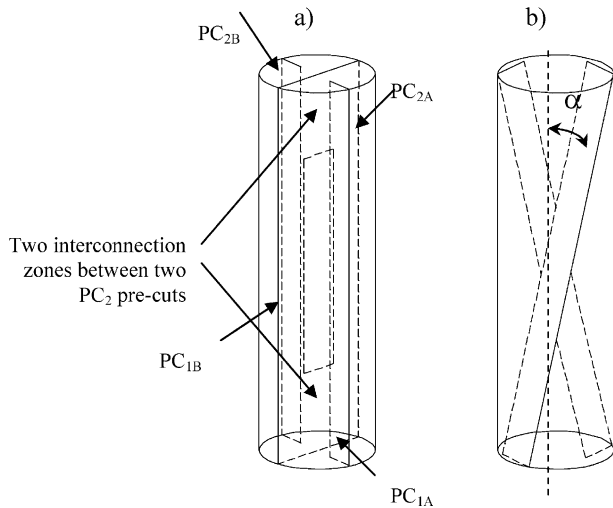


Fig. 3. The two types of pre-cuts. (a) The cut consists of two pairs of pre-cuts (PC_1 and PC_2) parallel to the vertical axis. The PC_1 pair was normally oriented to PC_2 . PC_{1A} and PC_{1B} are the first and the second pre-cuts, respectively, of the first pair PC_1 , while PC_{2A} and PC_{2B} are the first and the second pre-cuts, respectively, of the second pair PC_2 . PC_{2A} and PC_{2B} are interconnected at the top and bottom ends of the samples. Depths of interconnection zone are 30 mm at each end of the sample. (b) The second type of cut consists of two pre-cuts inclined (crosswise) to the vertical axis. Both pre-cuts create the same inclination angles α to the vertical axis. For a more detailed explanation of the inclination angle, see text.

perturbation creating the EMR was limited by this crack width (since at both sides of the crack atomic movements are restricted), the frequency should be given by:

$$\omega = \frac{\pi v_R}{b} \quad (4)$$

where v_R is the Rayleigh wave speed (Frid et al., 2003).

1.4. Objectives of the present study

The inducement of axial splitting is thought to be a relevant simulator of joint formation (e.g. Engelder et al., 1993, p. 141). In the present study we introduce a new technique for the inducement of both longitudinal splitting and en échelon fringes in glass. We intend to explore the loading conditions that induce en échelon segments alone, axial split alone, and combined segmentation and longitudinal splitting. Particularly, we shall try to simulate tensile longitudinal splitting that forms after joint fringes. Thus, we expect that our experiments will contribute to the understanding of geological fractures from both fracture mechanics (mixed mode I and III loading and en échelon segment) and rock mechanics (axial splitting) points of view. The new results are expected to improve our understanding of rapid joint formation, particularly in dynamically fractured granites during cooling conditions (Bahat et al., 2001a, 2002, 2003).

2. Experimental details

2.1. Experimental equipment and method

A load frame (TerraTek press model FX-S-33090; axial compression up to 450 MPa; stiffness 5×10^9 N/m) was used for the measurement. It is combined with a closed-loop servocontrol (linearity 0.05%), which is used to maintain a constant axial piston rate of displacement. The load was measured with a load cell (LC-222M; maximum capacity 220 kN, linearity 0.5% full scale). The axial cantilever set (strain range about 10%; linearity 1% full scale) enables us to measure sample strain along the samples' vertical axis. Each sample was uniaxially loaded by an axial constant strain rate of 1×10^{-5} s $^{-1}$.

A magnetic one-loop antenna (EHFP-30 Near Field Probe set, Electro-Metrics Penril Corporation) 3 cm in diameter was used for the detection of the EMR. It is wound within a balanced Faraday shield, so that its response to external electric fields is vanishingly small. A low-noise micro-signal amplifier (Mitek Corporation Ltd, frequency range from 10 kHz to 500 MHz, gain 60 ± 0.5 dB, noise level 1.4 ± 0.1 dB throughout) and analog-to-digital converter connected to a triggered PC completed the detection equipment (Rabinovitch et al., 1998, 1999; Frid et al., 1999).

2.2. Sample preparation

This study focused on cylindrical samples of soda-lime glass (10 cm in length and 3 cm in diameter). The density of all investigated samples was $2.6 \pm 0.01 \times 10^3$ kg/m 3 . Glass is a useful material for experimentation (Sommer, 1969), but it is a very strong one (uniaxial strength of glass is 750–900 MPa (Rous, 1966)).

A range of depths and geometries of specimen pre-cuts was tried. We found that it was necessary for cuts to be at least 10 mm deep before specimen failure occurred. Our preliminary results enabled us to find two basic types of pre-cuts (Fig. 3), which we could use for quantitative investigation.

The first type consists of two pairs of pre-cuts parallel to the sample vertical axis (Fig. 3a; Table 1, item 1), with one pair (PC_1) normally oriented to the other (PC_2). Two pre-cuts PC_{2A} and PC_{2B} of the second pair PC_2 were also interconnected at the top and bottom ends of the sample. The depth of the interconnection zones was 30 mm at both end parts of the sample. The second type consists of two pre-cuts inclined (crosswise) to the vertical axis (Fig. 3b; Table 1, items 2–7) creating about the same angle ($\alpha \pm 2^\circ$) with respect to the vertical axis (Fig. 4). Note, that for the first type of pre-cut $\alpha = 0^\circ$.

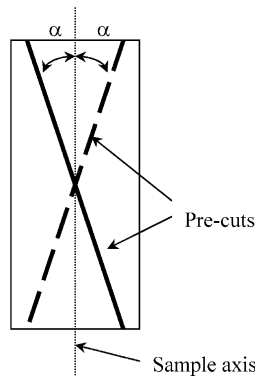


Fig. 4. Measurement scheme of the pre-cut angle of the second type cut. The pre-cut angle α is measured between the pre-cut end and the vertical axis of the sample.

3. Experimental results

3.1. Fractography

The fractographic investigation shows different failure behaviors that were obtained when differently pre-cut samples were tested. We concentrated on three failure styles: (a) axial split, (b) en échelon segments and (c) a combination of (a) and (b). The first failure style was noted only during failure of the sample of the first type of pre-cut (Fig. 3a, sample '1'; Table 1, item 1). The second failure style resulted from loading of sample of the second type of pre-cut (Fig. 3b) when compression was halted under low stress—55 MPa (sample '2'; Table 1, item 2). When samples of the second type of pre-cut were loaded up to their failure they yielded the third failure style behavior (samples '3–7'; Table 1, items 3–7). Hence, we concentrate here only on three samples (nos. 1, 2 and 5), one from each style of failure.

Sample '1' (first type of pre-cut, Fig. 3a). There is a longitudinal split 100 mm in length and 15 mm in width that developed between the one pair of precuts in specimen 1, without an en échelon segment.

Sample '2' (second type of pre-cut, Fig. 3b). There is only one fringe of en échelon segments in specimen 2 that developed next to the pre-cut without longitudinal split. The

segments vary from 1 to 5 mm in length (normal to the cylindrical axis) and from 0.5 to 3 mm in width (subparallel to the cylindrical axis).

Sample '5' (second type of pre-cut, Fig. 3b). Fig. 5 shows a representative fracture surface from sample 5. Note that we rotated the sample 90° clockwise into a horizontal position for a better fractographic description. The fracture may be characterized according to three lateral zones along the sample axis. A smooth central zone that is relatively less fractured (white color), which shows plumes at the two tips, indicating bilateral propagation from the center towards the two sample tips. Upper and lower fringes, above and below the central zone, are more intensely fractured into segmented cracks (gray-white), particularly the lower one. There is also a series of some 3–4 segmented cracks forming a distal-fringe that is oriented perpendicular to the sample axis at the right tip of the sample. The two plumes at the left tip and a plume at the right tip of the sample arrest at the fringes in areas of contact between the two. This is shown in Fig. 6a and e, which depict the enlarged left (experimental bottom) and right (experimental top) tips of the sample, implying that the fringes formed earlier than the central zone.

The lower fringe (Fig. 5) is fractured into some 12 segments that maintain approximately the same length (measured perpendicular to the sample axis). However, the fringe-cracks differ considerably in their widths, overall shapes and fractographies, indicating heterogeneous fracture processes along different directions of propagation in the fringes. Most neighbor cracks are separated from each other by straight fractures, but some are separated by curved boundaries (black shadows in various parts of Fig. 5). Fig. 6d and e shows a series of segments at the lower fringe. Several segments are marked by lateral striae that form orthogonal relations with sub-vertical undulations, implying that on individual segments fractures propagated sub-parallel to the sample side (and sample axis) and did not propagate vertically across the fringe as expected (Pollard et al., 1982). Thus, segments that cut striae (Fig. 6b) occurred after striae in some parts of the sample, while fractographies exhibited by some other segments imply that they developed after the separation of the cracks from each other, because

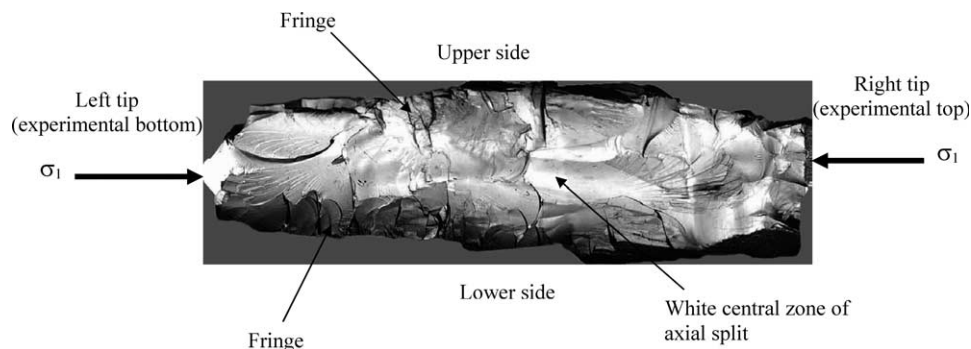


Fig. 5. A photograph of the fracture surface of glass sample number 5. Sample length is 100 mm. Note that: (a) sample was rotated 90° clockwise into a horizontal position; (b) arrows show the direction of the uniaxial compression and (c) three split branches close to the sample tips are indicated by three plumes.

a) Experimental top tip (Right tip in Fig. 5) d)

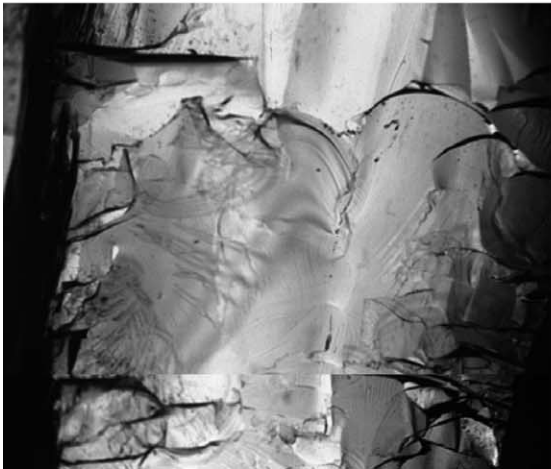


b)

e)



c)



Experimental bottom tip (Left tip in Fig. 5)

Fig. 6. Enlarged parts (a)–(e) (see text for explanation).

each segment exhibits different striae patterns. This seems to be a general fracture pattern except that some striae exhibit oblique fracture propagation (Fig. 6c and d) suggesting a rotation of the local stress field.

Two large segments, in the upper and lower fringes (Fig. 6b) are marked by ‘secondary mirrors’ that are surrounded by ‘secondary fringes’, such that the hackles in the fringes

propagate radially (Figs. 5 and 6b). A plume and undulations on one segment (Fig. 6e) propagate towards the sample center. These indicate independent fracture in various parts of the sample. Fig. 6a shows that the striae that ornament the distal fringe occur either along the length of the segments or inclined to them, repeating the analogous relationship observed in the lateral fringes. ‘Young’ scars

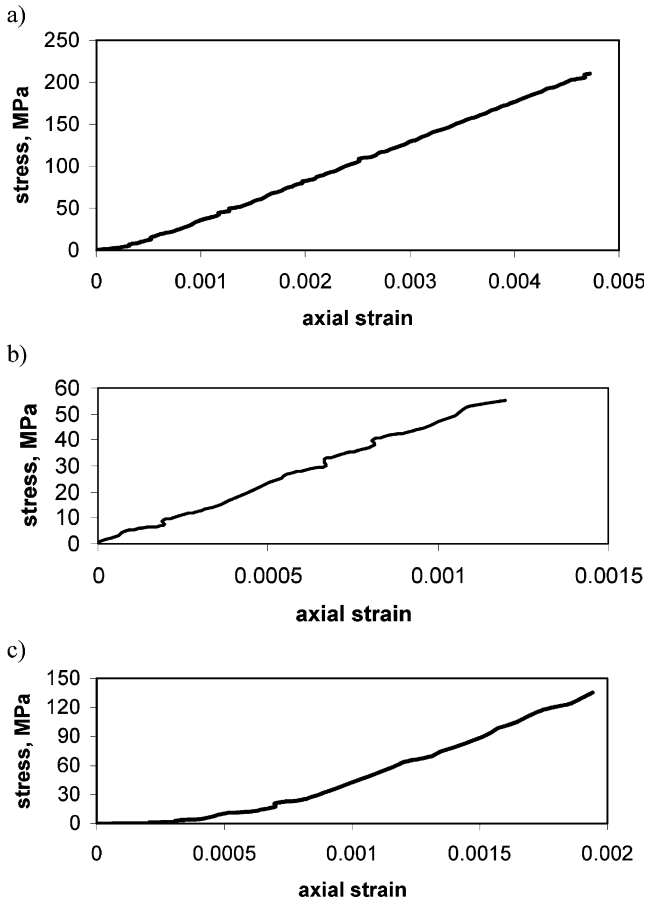


Fig. 7. (a) Stress–strain curve of sample ‘1’; (b) Stress–strain curve of sample ‘2’; (c) Stress–strain curve of sample ‘5’ (note scale differences).

like the one carving the second segment from the left (Fig. 6e) characterize various parts of the sample, possibly reflecting a late stage of stress relaxation.

Based on the above observations the sequence of events may be summarized from early to late events as follows. Heterogeneous fracture occurred along the fringes, such that lateral striae occurred before segmentation in some parts, while segments preceded striae in other parts. The separation of the en échelon segments and the lateral striae sub parallel to the sample axis suggest a minor tensile stress

parallel to the sample axis in certain parts of the fringes. Heterogeneous fracture also occurred in a fringe normal to the sample axis at the right tip of the sample. Longitudinal splitting initiated at the center and propagated bilaterally towards the two tips along the central zone of the sample. The large fracture surface shown in Figs. 5 and 6 was induced by the major tensile stress normal to the sample axis. Late microcracking at least partly formed upon stress relaxation.

One can see repetition of the various crack modes in an evolutionary manner in various samples given in Table 1 (from item 2 to items 3–7). In item 1 where $\alpha=0$ only splits occurred without segmentation.

3.2. Sample strength

3.2.1. Sample strength and pre-cut angle changes

Fig. 7a shows the stress–strain graph of the sample of the first type of pre-cuts (Table 1, sample 1). Fig. 7b shows the stress–strain graph of the sample of the second type of pre-cuts (Table 1, sample 2, having pre-cut angle $\alpha=12.5^\circ$), which was uniaxially loaded up to the time when first EMR signals, induced by the first cracks events, appeared (40–55 MPa).

Five other samples of the second type of pre-cuts (Table 1, samples 3–7, having pre-cut angle α between 6.5 and 50°) were uniaxially compressed up to their failure and all of them showed a strength of less than 200 MPa (Table 1). Fig. 7c shows the stress–strain curve of sample number 5 (Table 1, $\alpha=39^\circ$) while Fig. 8 shows that α of about $7 \pm 2^\circ$ yields a minimal sample’s strength.

3.2.2. Sample strength and twist angle of the longitudinal split

Our experimental results show that the fracture surfaces of the pre-cut samples (longitudinal splits) are twisted and quasi parallel to the échelon fringe planes. We designated the twist angle of the longitudinal split γ as the one formed by the two diagonal ends of the longitudinal split (at the upper and lower ends of the cylinder). To measure this angle, one top end of the longitudinal split TT_1 was oriented

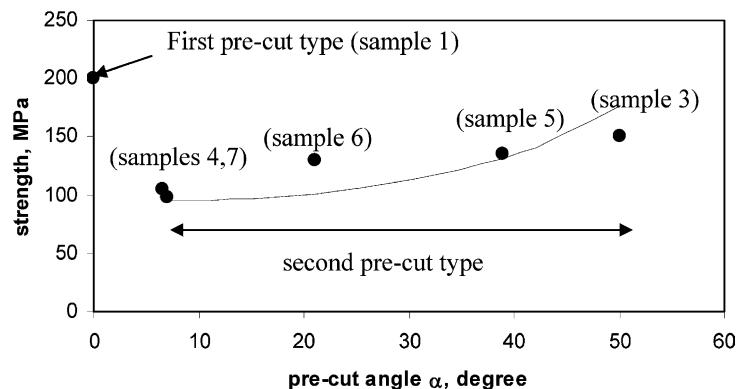


Fig. 8. The relation between the pre-cut angle α and sample strength (samples are described in Table 1). Full line—the theoretical strength (Eq. (5)).

Table 1
Sample properties and fracture characterization

Item	Sample number	Maximal stress (MPa)	Pre-cut type	Fracture style	Angle between pre-cut and sample axis α (°)	Twist angle γ (°)
1	2	3	4	5	6	7
1	1	200	1	Longitudinal split	0	0
2	2	55 ^a	2	En échelon segments	12.5	–
3	3	150	2	En échelon segments. Longitudinal split	50	85
4	4	98	2	En échelon segments. Longitudinal split	7	200
5	5	135	2	En échelon segments. Longitudinal split	39	105
6	6	130	2	En échelon segments. Longitudinal split	21	130
7	7	105	2	En échelon segments. Longitudinal split	6.5	210

^a Sample number 2 was not broken under compression—test was halted—see explanation in the text.

north-wise, and an angle between TT_1 and the diagonal bottom end TB_1 of the longitudinal split was clockwise measured. Fig. 9a shows the orientation of the glass sample relative to the compressive stress direction, while Fig. 9b shows a projection of the top and bottom tips on a common horizontal surface to measure the twist angle of the longitudinal split. Results of our measurements are summarized in Table 1 (column 7). The plot of these results (Fig. 9c) shows that the twist angle γ is zero when the angle between the pre-cuts is also 0° (first type of pre-cut). A pre-cut angle $\alpha = 7 \pm 2^\circ$ (second type of pre-cut) yielded the maximal twist angle while an increase of α from 7 to 50° excited a gradual decrease of twist angle γ . Thus, the γ vs. α curve has a maximum at $\alpha = 7 \pm 2^\circ$ that is close to the maximum deviation of splits from the sample axis in conventional triaxial tests (Holzhausen and Johnson, 1979; Bahat et al., 2001a), and then decreases with the increase of local compression perpendicular to the sample axis.

3.3. EMR sequences

Our results show that each segment emits an EMR burst that appears in the record as a string of several individual EMR pulses (e.g. Fig. 10a). In our previous papers (Rabinovitch et al., 1998, 1999, 2000; Frid et al., 2000, 2003; Bahat et al., 2001b) we elaborated on the method by which we correlate EMR pulses with crack appearances according to their lengths, widths and areas and according to their mode of fracture, i.e. tensile or shear. Thus, the number of EMR strings in this paper corresponds to the number of en échelon segments. For example, during the loading of sample '2', seven en échelon segments were formed between stresses of 40 and 55 MPa, and correspondingly seven EMR strings were registered. The time intervals

between EMR stings were between 0.5 ms and 1 s. Each EMR string here consisted of several short individual EMR pulses with time pauses between pulses of 0.1 to 0.3 ms. An example of a single EMR string is shown in Fig. 10a, while Fig. 10b shows an example of a short individual EMR pulse within a string.

As can be inferred from Eqs. (3) and (4), the ratio T'/ω is proportional to the crack area $\ell \times b$, where the proportionality coefficient depends on the crack propagation velocity. Calculation of Rayleigh speed (from the glass elastic properties observed in our compression tests) shows it to be about 3000 m/s. The crack propagation velocity, which is usually around one-third Rayleigh speed (Fineberg and Marder, 1999; Boundet and Ciliberto, 2000), can be estimated to be about 1000 m/s in the fringe zone. This is a much faster fracture velocity than obtained by Muller and Dahm (2000), who found a trend of fracture velocity decrease at the fringe.

Estimation of crack areas from EMR parameters shows that each short EMR pulse (Fig. 10b) is induced by a crack area of about of 0.01–0.1 mm², while the total areas calculated by summing up of all sub-areas of a complete EMR string (e.g. Fig. 10a) are in the range 1–10 mm². The latter values agree with the dimensions of the en échelon segments. We cannot assert that each short EMR pulse observed in a particular EMR string is induced by a specific en échelon segment. However, the qualitative fit between the number of EMR strings and the overall en échelon segments indicates that each en échelon segment is composed of several short crack events. Further research should establish the role of the micro-crack (0.01–0.1 mm²) propagation at the outset of the larger en échelon (1–10 mm²) growth.

The number of lengthy EMR pulses (Fig. 2) agrees with the number of longitudinal splits created during the sample's deformation. One lengthy EMR pulse was

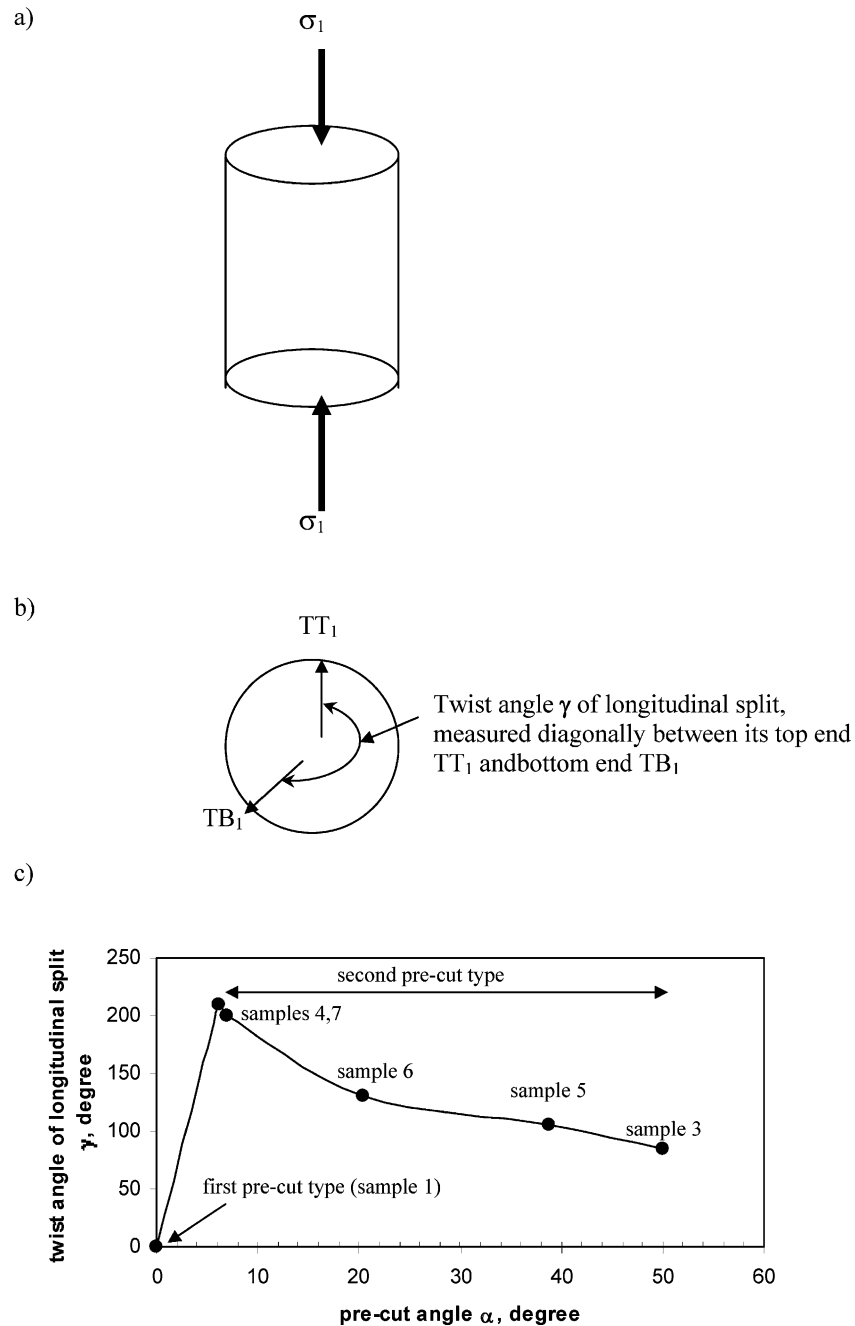


Fig. 9. (a) The orientation of the glass sample relative to the compressive stress direction. (b) Projection of the top and bottom tips of the glass sample on a common horizontal surface to measure the twist angle of longitudinal split γ : the top end of the longitudinal split TT_1 was oriented north-wise, and the angle between this top end and the diagonal bottom end, TB_1 , of the longitudinal split was measured clockwise. (c) The relation between the twist angle γ of longitudinal split and the pre-cut angle α .

measured during the loading of sample '1' (Table 1). This pulse corresponds to one axial split similar to the three split branches shown in Fig. 5.

Two types of EMR signals were measured during sample '5' (Table 1) loading: short ones and lengthy ones. Short signals were picked up at stresses between 45 and 50 MPa and were composed of the EMR strings mentioned above. The first lengthy EMR signal was registered at 60 MPa, and about 1 min later two other lengthy signals were measured with an interval of 11 s between them.

The measured fracture widths show a good fit with Eq. (4), while calculated fracture lengths by Eq. (3) appear to be less by a factor of two from the measured ones. This result possibly indicates that during the final stage of failure in the pre-cut sample, fractures propagated in a 'blast-wise' manner and hence fracture speed was much larger than the estimated 1000 m/s (about Rayleigh speed), i.e. that the formation of the longitudinal split was associated with a sudden release of energy that resulted in an abrupt jump to high terminal crack velocity.

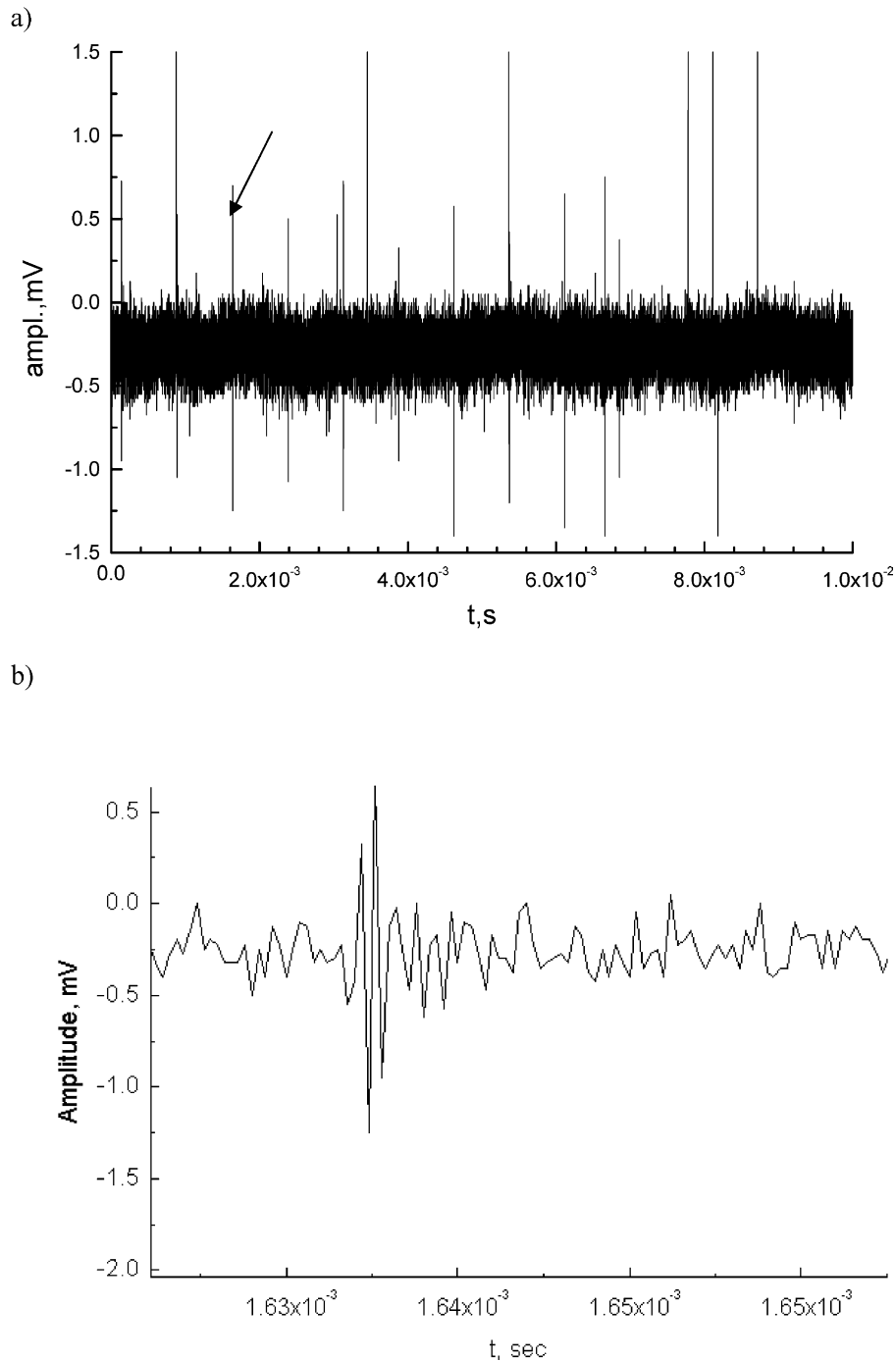


Fig. 10. EMR string (a) consisting of 16 short EMR pulses with amplitudes higher than 0.25 mV; arrow shows short EMR pulse enlarged in (b).

4. Discussion

4.1. Failure and stress distribution

Samples of the first and second pre-cut types responded to completely different local stress conditions. Samples of the first pre-cut type failed under simple longitudinal splits, normal to the extension stress. On the other hand, samples of the second pre-cut type failed in a complex fracture. The remote compression maintained its uniaxial direction in the

latter, but the local principal directions rotated throughout the fracture process. Generally, the major principal tensile stress was normal to the fracture surface (shown in Fig. 5) during segment and longitudinal splitting, and a minor tensile principal stress paralleled the sample axis along the fringes. The former is demonstrated by the predominant tensile surface along the sample, and the latter is shown by the separation of the segments from each other in Figs. 5 and 6 (note the wide black shadows between segments). However, the minor tensile principal stress was partly

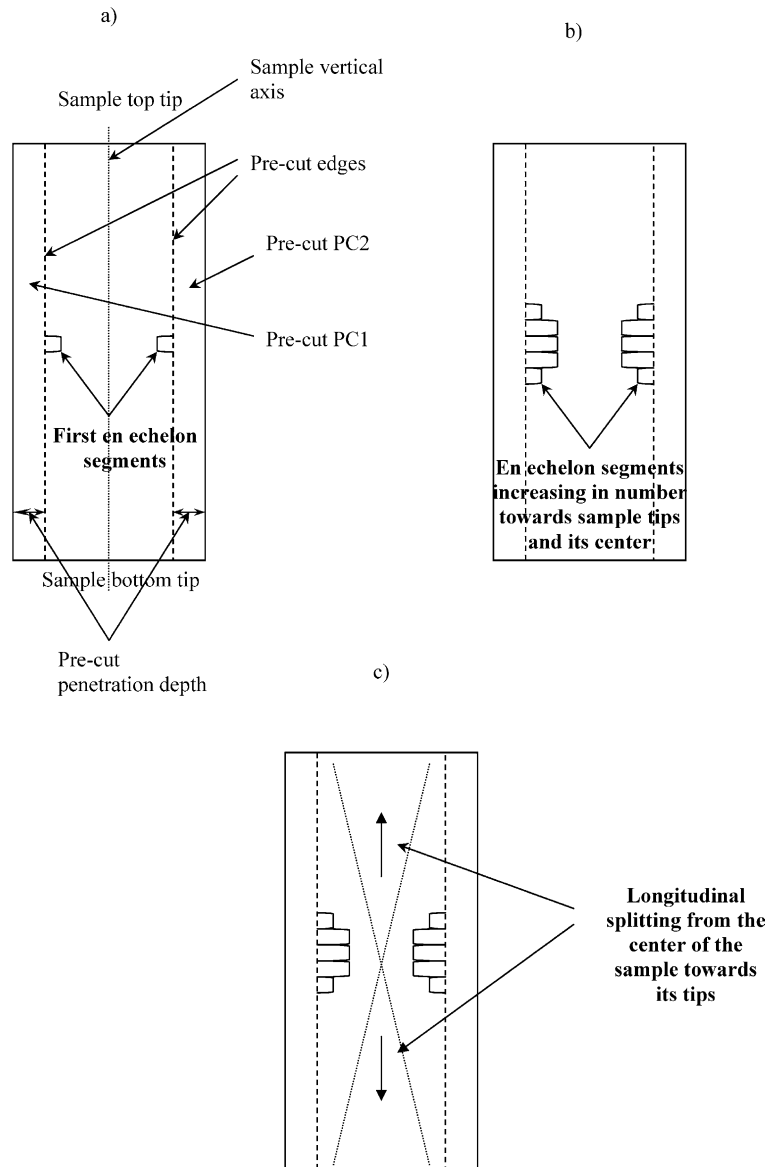


Fig. 11. A flat 2D projection of the 3D (twisted) surface created during failure of glass samples of the second type of pre-cut. The fracture process consists of three main stages: (a) nucleation of an en échelon segment at the edges of both pre-cuts (PC₁ and PC₂) about the middle of the sample height; (b) an increase of the en échelon dimensions and number, towards sample center and along both edges of pre-cuts towards sample tips; (c) propagation of axial splits from en échelon fringes (from about the mid sample height) to sample tips (see arrows) along sample vertical axis.

converted locally to compression as demonstrated by the lateral striae on the segments (Fig. 6d and e). Occasional inclined and curved striae record stages of principal stress rotation in local fields (in the upper fringe of Fig. 6b and c).

4.2. Failure mechanism of glass samples

Both fractographic and EMR results show that the failure mechanism of the second pre-cut type may be described in the following manner. The 'en échelon' segment begins under stresses of the order of 40–55 MPa at the edges of the couple of pre-cuts in the central zone of the sample

(Fig. 11a). Comparison of fracture surfaces of crosswise pre-cut sample (second pre-cut type) that failed under different loads shows that an increase of external load results in the increase of the number of en échelon cracks in two perpendicular directions: from the edges of the two pre-cuts towards the center of the sample, and along the pre-cuts (Fig. 11b). An additional increase of the vertical load excites a longitudinal split (Fig. 11c).

The en échelon segment is formed by a cooperative action of the uniaxial load from the press piston and an internal stress due to the crosswise shape of the pre-cuts. This crosswise shape causes a formation of internal mixed modes I and III on the edges of the couple of pre-cuts,

exciting crack propagation along, and perpendicular to, the sample pre-cuts. A rapprochement of the two groups of segments from the pre-cuts towards the center of the sample forms a condition of stress concentration there and hence leads to the nucleation of a split that propagates in a trend that sub parallels the sample axis. Twisting is allowed between 0 and 8° (Holzhausen and Johnson, 1979; Bahat et al., 2001b) from the sample axis. This sub parallelism occurs under a stress now larger than the one inducing the en échelon segments (Fig. 8).

4.3. Sample strength

To understand the increase of strength of samples of the second type of pre-cut we employed the stress analysis of samples with a plane of weakness. Since the en échelon formations begin independently from each pre-cut and are symmetrical with respect to the glass cylinder axis we assume that the stress analysis can be carried out for a sample with a single plane of weakness. The strength of such a sample is (see e.g. Jaeger, 1964):

$$\sigma = \frac{2S_0 \cos\phi}{(\sin(2\alpha + \phi) + \sin\phi)} \quad (5)$$

where α is the angle of the plane of weakness with respect to the main stress axis, ϕ is the angle of internal friction and S_0 is the glass cohesion.

The ratio of the compressional to the tensional strength of glass varies between 8 and 10 implying that the value of the angle of the internal friction varies between 51 and 55°. For the mean value of this ratio (9) the angle of internal friction is 53°. The strength of glass, as noted above, is between 750 and 900 MPa, highly dependent on the degree of polishing. Since our samples were highly polished we use the highest strength (900 MPa) here.

Fig. 8 shows the changes of sample strength according to Eq. (5). Comparison with experimental results is quite good.

4.4. Comparison of the present fringes to others in geological outcrops

Our comparison relates to the fracture modes, cracking in the fringes and longitudinal splitting.

4.4.1. Fringes

The fringes that appear in Figs. 5 and 6 partly resemble hackle-fringes that were recently identified on joint surfaces cutting granites (Bahat et al., 2001a, 2002, 2003). The resemblance includes the non-uniform sizes of the fringes of cracks and their wide variations in shapes and their overlapping styles. The resemblance is also in the appearance of 'secondary mirror' and 'secondary fringe' (Figs. 5 and 6b). The hackle-fringes on fractured glass surfaces (Kerckhoff, 1975) and those surrounding joints in granites were interpreted to represent dynamic fracture

under high stress intensity conditions and rapid fracture (Bahat et al., 2001a). The present fracture morphologies clearly resulted from rapid fracture that was induced by remote compression under dynamic conditions. Hence, this resemblance could be expected.

However, there is also a notable difference between the segments in Fig. 5 and the hackle-fringes that occur by conventional tensile (or bending) experiments (e.g. Bahat et al., 1982) and in granites. A recent study shows that in a given area of fringe on a joint cutting granite, larger new areas form in the transition from mirrors to hackle-fringes, under mode I than in the transition from mirrors to en échelon-fringes, under mixed modes I and III. The reason for the difference in new area is that the change in mode I loading to mixed mode I+III reduces the amount of energy that is spent in forming new fracture areas (Bahat et al., 2002). The separation of the segments rather than their overlapping in the fringes of sample 5 shows that only a limited new area was formed in the fringes. Apparently, a transient, local, minor tension in the fringes that paralleled to the sample axis separated the segments, in addition to the existing major tensile direction normal to the sample axis that is manifested by the plumes. Separation of segments is not identified in the granite, but this effect characterizes fringes of discoid joints that occur in chalks (Bahat, 1997, Fig. 6f) and in other rocks. This separation was assigned to local pure tension that was extended on certain parts of the discoid. We suggest that the above difference relates to the development of local, transient (minor tension) in the fringes of sample 5 and the discoid joints, compared with a remote tension that induced hackle-fringes in the granites.

The same sample twist that caused the formation of the lateral fringes (Fig. 5) may have been the reason for the occurrence of the distal fringe (Fig. 6a). The two large lateral cracks formed at the upper left side of the sample (Fig. 5), were possibly induced by this twist as well. Thus, it appears that the crack-segment in sample '5' represents fringes that possess characteristics from both en échelon fringes and hackle-fringes. Previous fracture inducements leading to en échelon-fringes resulted from experimental conditions of remote mixed mode I+III (Sommer, 1969), while hackle-fringes were induced by remote tension (Bahat et al., 1982; Rabinovitch et al., 2000a,b,c). The present inducement on the other hand, took place under experimental conditions of remote compression, combined with local twisting. Further extension of studies on dynamic geological fracture (in outcrop scale, Bahat et al., 2001a, 2002) may possibly encounter fracture processes of the kind presented in this study.

4.4.2. Longitudinal splitting

Generally, longitudinal splits do not start from the sample center because this is a zone of great strength. They often initiate from the sample tip boundaries and propagate axially to the center. Weakening of the sample center can, however, initiate longitudinal split there by buckling

(Holzhausen and Johnson, 1979). Such a weakening may be tensile (Bahat et al., 2001a) or, as in the present study, by an échelon segment as follows. This study demonstrates the new technique of initiating longitudinal split in the sample center: Under large twist angles between inclined pre-cuts, combined with uniaxial compression, an échelon segmentation starts from the inner ends of the pre-cuts and propagates to the center. The sample center becomes weak, enabling the longitudinal splits to initiate there and propagate bilaterally to the two tips along two limited zones.

Acknowledgements

This research was supported by the Israel Science Foundation (No. 93/02-1) and Earth Sciences Administration (Ministry of Energy and Infrastructure, No. 22/17-008). For important technical help, we owe thanks to Vyacheslav Palchik and Dina Frid.

References

- Bahat, D., 1986. Joints and en échelon cracks in middle Eocene chalks near Beer-Sheva, Israel. *Journal of Structural Geology* 8, 181–190.
- Bahat, D., 1997. Mechanisms of dilatant en échelon crack formation in jointed layered chalks. *Journal of Structural Geology* 19, 1375–1392.
- Bahat, D., Bankwitz, P., Bankwitz, E., 2001a. Changes of crack velocities at the transition from the parent joint through the en échelon fringe to a secondary mirror plane. *Journal of Structural Geology* 23, 1215–1221.
- Bahat, D., Bankwitz, P., Bankwitz, E., 2003. Pre-uplift joints in granites: evidence for sub-critical and post-critical fracture growth. *Geological Society of America Bulletin* 115, 148–165.
- Bahat, D., Leonard, G., Rabinovitch, A., 1982. An analysis of symmetric fracture mirrors in glass bottles. *International Journal of Fracture* 18 (1), 29–38.
- Bahat, D., Rabinovitch, A., Frid, V., 2001b. Fracture characterization of chalk in uniaxial and triaxial tests by rock mechanics, fractographic and electromagnetic radiation (EMR) methods. *Journal of Structural Geology* 23, 1531–1547.
- Bahat, D., Rabinovitch, A., Frid, V., 2004. Tensile fracture in rocks. Springer-Verlag, Heidelberg, 570pp.
- Bahat, D., Bankwitz, P., Bankwitz, E., Rabinovitch, A., 2002. Comparison of the new fracture areas created by the formation of en échelon and hackle fringes on joint surfaces. *Zeitschrift fuer Geologische Wissenschaften* 30, 1–12.
- Bankwitz, P., 1965. Über klufte. I beobachtungen im thuringischen schiefergebirge. *Geologie* 14, 241–253.
- Boundet, J.F., Ciliberto, S., 2000. Interaction of sound with fast crack propagation: an equation of motion for the crack tip. *Physica D* 142, 317–345.
- Cook, M.L., Pollard, D.D., 1996. Fracture propagation paths under mixed mode loading within rectangular blocks of polymethyl methacrylate. *Journal of Geophysical Research* 101, 3387–3400.
- Cress, G.O., Brady, B.T., Rowell, G.A., 1987. Sources of electromagnetic radiation from fracture of rock samples in the laboratory. *Geophysical Research Letters* 14, 331–334.
- Engelder, T., Fischer, M.P., Gross, M.R., 1993. Geological aspects of fracture mechanics. A short course manual note. Geological Society of America, Annual Meeting, Boston, Massachusetts.
- Fineberg, J., Marder, M., 1999. Instability in dynamic fracture. *Physics Reports* 313, 1–108.
- Frid, V., Rabinovitch, A., Bahat, D., 1999. Electromagnetic radiation associated with induced triaxial fracture in granite. *Philosophical Magazine Letters* 79, 79–86.
- Frid, V., Bahat, D., Goldbaum, J., Rabinovitch, A., 2000. Experimental and theoretical investigation of electromagnetic radiation induced by rock fracture. *Israel Journal of Earth Sciences* 49, 9–19.
- Frid, V., Rabinovitch, A., Bahat, D., 2003. Fracture induced electromagnetic radiation. *Journal Physica D* 36, 1620–1628.
- Gol'd, R.M., Markov, G.P., Mogila, P.G., 1975. Pulsed electromagnetic radiation of minerals and rock subjected to mechanical loading. *Physics Solid Earth* 7, 109–111.
- Gramberg, J., 1965. Axial cleavage fracturing, a significant process in mining and geology. *Engineering Geology* 1, 31–72.
- Hodgson, R.A., 1961. Classification of structures on joint surfaces. *American Journal of Science* 259, 493–502.
- Holzhausen, G.R., Johnson, A.M., 1979. Analyses of longitudinal splitting of uniaxially compressed rock cylinders. *International Journal of Rock Mechanics Mining Sciences & Geomechanical Abstracts* 16, 163–177.
- Jaeger, J.C., 1964. *Elasticity Fracture and Flow*. Butler and Tanner Ltd, London, 212pp.
- Kerckhoff, F., 1975. Bruchmechanische analyse von schadensfallen und glasern. *Glastechnische Berichte* 48, 112–124.
- Khatiashvili, N., 1984. The electromagnetic effect accompanying the fracturing of alkaline halide crystals and rocks. *Physics Solid Earth* 20, 656–661.
- Muller, G., Dahm, T., 2000. Fracture morphology of tensile cracks and rupture velocity. *Journal of Geophysical Research* 105, 723–738.
- Nitsan, V., 1977. Electromagnetic emission accompanying fracture of quartz-bearing rocks. *Geophysical Research Letters* 4 (8), 333–336.
- O'Keefe, S.G., Thiel, D.V., 1995. A mechanism for the production of electromagnetic radiation during fracture of brittle materials. *Physics of the Earth and Planetary Interiors* 89, 127–135.
- Ogawa, T., Oike, K., Miura, T., 1985. Electromagnetic radiation from rocks. *Journal of Geophysical Research* 90 (d4), 6245–6249.
- Pollard, D.D., Segall, P., Delaney, P.T., 1982. Formation and interpretation of dilatant échelon cracks. *Geological Society of America Bulletin* 93, 1291–1303.
- Rabinovitch, A., Frid, V., Bahat, D., 1998. Parametrization of electromagnetic radiation pulses obtained by triaxial fracture in granite samples. *Philosophical Magazine Letters* 5, 289–293.
- Rabinovitch, A., Frid, V., Bahat, D., 1999. A note on the amplitude–frequency relation of electromagnetic radiation pulses induced by material failure. *Philosophical Magazine Letters* 79, 195–200.
- Rabinovitch, A., Belizovsky, G., Bahat, D., 2000a. Origin of mist and hackle patterns in brittle fracture. *Physical Review B* 61, 968–974.
- Rabinovitch, A., Zlotnikov, R., Bahat, D., 2000b. Flaw length distribution measurement in brittle materials. *Journal of Applied Physics* 87, 7720–7725.
- Rabinovitch, A., Frid, V., Bahat, D., Goldbaum, J., 2000c. Fracture area calculation from electromagnetic radiation and its use in chalk failure analysis. *International Journal of Rock Mechanics Mining Sciences & Geomechanical Abstracts* 37, 1149–1154.
- Rabinovitch, A., Frid, V., Bahat, D., Goldbaum, J., 2003. Decay mechanism of the fracture induced electromagnetic pulses. *Journal of Applied Physics* 93 (9), 5085–5090.
- Rous, B., 1966. *Sklo v electronice*, PRAHA (Statni Nakladatelstvi technicke literatury), 355pp.
- Sommer, E., 1967. Das bruchverhalten von rundstaben aus glas im manteldruckversuch mit uberlagerte zugspannung. *Glastechnische Berichte* 40, 304–307.
- Sommer, E., 1969. Formation of fracture 'lances' in glass. *Engineering Fracture Mechanics* 1, 539–546.
- Twiss, R.J., Moores, E.M., 1992. *Structural Geology*. Freeman, New York.
- Ueda, S., Al-Damegh, K.S., 1999. Evaluation of VAN method. Atmospheric and Ionospheric Electromagnetic Phenomena associated with Earthquakes. 53–69.

- Urusovskaja, A.A., 1969. Electric effects associated with plastic deformation of ionic crystals. *Soviet Physics-Uspokhi* 11, 631–643.
- Warwick, J.W., Stoker, C., Meyer, T.R., 1982. Radio emission associated with rock failure: possible application to the Great Chilean Earthquake of May 22, 1960. *Journal of Geophysical Research* 87 (b4), 2851–2859.
- Yamada, I., Masuda, K., Mizutani, H., 1989. Electromagnetic and acoustic emission associated with rock fracture. *Physics of the Earth and Planetary Interiors* 57, 157–168.
- Younes, A.I., Engelder, T., 1999. Fringe cracks: key structures for the interpretation of the progressive Alleghanian deformation of the Appalachian Plateau. *Geological Society of America Bulletin* 111, 219–239.